Design and implementation of linear-quadratic-Gaussian stability augmentation autopilot for unmanned air vehicle

C.-S. Lee, **p4897702@mail.ncku.edu.tw**
F.-B. Hsiao and **fbhsiao@mail.ncku.edu.tw**
S.-S. Jan **ssjan@mail.ncku.edu.tw**
Institute of Aeronautics and Astronautics
National Cheng Kung University
Tainan City
Taiwan

ABSTRACT

The linear-quadratic-Gaussian (LQG) control synthesis has the advantage of dealing with the uncertain linear systems disturbed by additive white Gaussian noise while having incomplete system state information available for control-loop feedback. This paper hence explores the feasibility of designing and implementing a stability augmentation autopilot for fixed-wing unmanned air vehicles using the LQG approach. The autopilot is composed of two independently designed LQG controllers which control the longitudinal and lateral motions of the aircraft respectively. The corresponding linear models are obtained through a system identification routine which makes use of the combination of two well-established identification methods, namely the subspace method and prediction error method. The two identification methods complement each other well and this paper shows that the proposed system identification scheme is capable of attaining satisfactory state-space models. A complete autopilot design procedure is devised and it is shown that the design process is simple and effective. Resulting longitudinal and lateral controllers are successfully verified in computer simulations and actual flight tests. The flight test results are presented in the paper and they are found to be consistent with the simulation results.

NOMENCLATURE

A,B,C,H	state space system matrices
h	altitude
J	cost function
K	optimal feedback gain in linear-quadratic regulator (LQR)
k	discrete system time step
L	optimal estimator gain in Kalman filter
L,M,N	components of applied aerodynamic moment vector in body axes
L_c,M_c,N_c	moment derivative with respect to variable C
N	total number of data
$Oxyz$	body axes
p,q,r	components of angular velocity vector in body axes
Q,R	LQR weighting function
$\boldsymbol{Q_k R_k}$	Kalman filter weighting function
$\bar{\mathbf{Q}}$	altered Q
u	input vector
u_{iM}	maximum allowable deviation in component ui
u,v,w	components of translational velocity vector in body axes
V	aircraft total velocity
v	measurement noise vector
w	process noise vector
x	system state vector

Paper No. 3377. Manuscript received 24 November 2008, revised version received 2 March 2009 accepted 23 March 2009.

https://doi.org/10.1017/S0001924000002955 Published online by Cambridge University Press

$\hat{\mathbf{x}}$	predicted state sequence or Kalman state sequence
X, Y, Z	components of applied aerodynamic force vector in body axes
X_c, Y_c, Z_c	force derivative with respect to variable C
$\mathbf{y}$	output state vector
$\hat{y}$	predicted output response
$\mathbf{z}$	performance output
z_{iM}	maximum allowable deviation in component z_i
α	angle-of-attack
β	angle-of-sideslip
Δ	perturbation from trim value
$\delta_e,\delta_a,\delta_r$	deflection angle of elevator, aileron, rudder
ξ	difference between predicted output and the measured output
ϕ,θ,ψ	Euler angles (bank, pitch, yaw)

Abbreviations

AHRS	attitude and heading reference system
CF	compact flash
CFD	computational fluid dynamics
COM port	communication port
GCS	ground control station
GPS	global positioning system
LPV	linear parameter varying
LQG	linear-quadratic-Gaussian
LQR	linear-quadratic regulator
MEMS	micro-electro-mechanical system
NRM	norm
OBC	onboard computer
PEM	prediction error method
PWM	pulse-width modulation
RMRL	remotely piloted vehicle and microsatellite research laboratory
UAV	unmanned air vehicle

1.0 INTRODUCTION

As of October 2006, it is estimated that the coalition Unmanned Air Vehicle (UAV) systems had flown almost 400,000 hours in support of Operations Enduring Freedom and Iraqi Freedom in recent high profile international warfare[1]. That is a huge increment compared to 100,000 flight hours as of September 2004[2]. The importance and contributions of the UAV systems to the armed forces would only continue to grow in the future for the potential applications and benefits of UAV systems can never be overemphasised. Driven by the need to fulfill various military mission requirements, the UAV-related technologies have been progressing in an astounding speed over recent decades. The ultimate goal is commonly perceived as achieving the level of autonomy of the UAV to the state where little or no human intervention is needed during an entire mission.

In the mean time, the applications of UAV systems in the civil grounds have gradually been picking up pace as well. The situation is further stimulated by the advancement in the computing and Micro-Electro-Mechanical Systems (MEMS) technology which produce smaller, faster and more efficient onboard avionics systems featuring miniature sensors and high performance microcontrollers. This has indirectly renewed the research interests in a variety of topics in aeronautical engineering such as airframe design, composite materials, flight control systems, miniature avionics, etc. since it is feasible and affordable for a small-scale university laboratory to build and maintain a UAV system, instead of a manned aircraft. Currently, there are a wide variety of UAV systems under development, including fixed-wing, rotorcraft, tail-sitter, tilt-rotor, *et cetera*. This paper focuses on the design and implementation of the automatic flight control system (autopilot) of the fixed-wing, conventional type unmanned air vehicle. Surprisingly, not many papers turned up in the open literature pertaining to the research and development on the automatic controls exclusive of UAV systems. Linear-quadratic design synthesis, especially the linear-quadratic regulator (LQR) control was adopted successfully by Montgomery[3] and Cho *et al*[4]. Interestingly, both UAV systems used a single GPS (Global Positioning System) receiver as the primary sensor to achieve automatic flights. The Stanford University's Dragonfly project group has been investigating the application of advanced control systems on UAV for quite some time, especially in the area of nonlinear control such as discrete disturbance control[5], sliding mode control[6], and discrete-time dynamic inversion[7]. Nevertheless, the above-mentioned advanced control approaches are only possible if high fidelity nonlinear models of the aircraft are available. Moreover, resulting controllers require significant computing power of the onboard system due to the more complex control algorithm.

On the other hand, other research teams have been exploring the feasibility of utilising robust control theory on UAV, for instance AlSwailem[8] and Natesan *et al*[9]. AlSwailem[8] applied robust loop-shaping methodology on the Cranfield A3 Observer UAV while Natesan *et al*[9] designed a longitudinal controller using μ -synthesis approach based on simplified linear parameter varying (LPV) model of a generic model representative of the class of UAVs that operate at low Reynolds number. Both studies provided simulation results only since robust control typically requires high data sampling rate and results in complex control algorithm. This made robust control theory somewhat difficult to be realised on a relatively small UAV system. Similar conclusions may be drawn on the combined adaptive autopilot reported by Andrievsky and Fradkov[10]. The adaptation algorithm provides the prescribed dynamic properties of the attitude control system for various flight conditions of the UAV but the paper fell short of substantiating the simulation results with flight test data.

In light of the above discussions, the LQR control seems to be a promising candidate for UAV's autopilot design. It is attractive in the sense that the control theory is well-established mathematically and the resulting control law is simple and elegant. This enables it to be easily implemented on UAV system such as those demonstrated in Montgomery[3] and Cho *et al*[4]. However, the biggest drawback of LQR control is the requirement of real-time full state measurement which is often unavailable in practice. This paper therefore attempts to explore the feasibility of adopting the linear-quadratic-Gaussian (LQG) control methodology on the automatic flight controls of fixed-wing UAVs. As a first step, a stability augmentation autopilot based on LQG control approach will be implemented on the Spoonbill UAV and further validated in series of flight tests. The Spoonbill UAV system is the latest brainchild of the Remotely Piloted Vehicle and Microsatellite Laboratory (RMRL) of National Cheng Kung University (NCKU), Taiwan who has been working on automatic flight control system of UAV since the beginning of this millennium. The laboratory is currently developing an entirely new UAV system under a long endurance UAV project called the Spoonbill project[11]. If successful, the final outcome of the project would be a long endurance UAV system capable of performing fully automatic flight mission from takeoff to landing. Essentially, this paper represents the early stage effort which constitutes a fundamental portion of the work laid out in the blueprint of the Spoonbill project. The background of the Spoonbill project is briefly introduced in the next section.

The remaining parts of this paper are organised as follows: Section 2 describes the air vehicle and onboard avionics system of the Spoonbill UAV system while Section 3 elaborates aircraft modeling and the system identification efforts. The identification routines, identification algorithms and data smoothing techniques are introduced as well. At the end of this section, identification results for both longitudinal and lateral model are presented. Next, the design procedures of the stability augmentation autopilot based on LQG control laws are described in Section 4. The resulting controllers in longitudinal and lateral motions are validated in computer simulations and ultimately in actual flight tests (Section 5). To wrap things up, the last section concludes the outcome of this paper and outlines some future works that are relevant to the framework of this paper.

https://doi.org/10.1017/S0001924000002955 Published online by Cambridge University Press

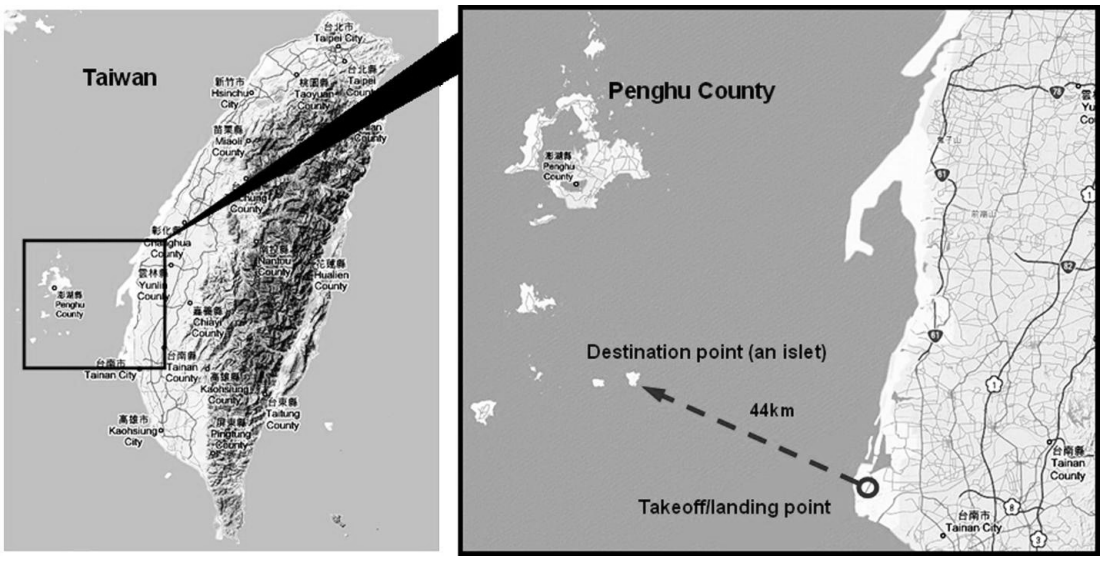


Figure 1. Cross-sea flight challenge from west coast of Taiwan to offshore Penghu County.

1.1 Background of Spoonbill project

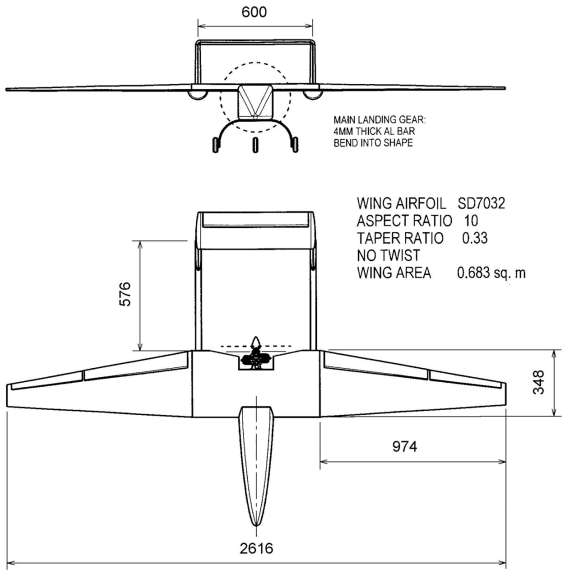
The Spoonbill project was established in the end of 2006 following the successful cross-sea flight demonstration of RMRL's previous UAV system, the SWAN[12,13]. The Spoonbill UAV was named after a type of Taiwanese migrant bird, the Black-faced Spoonbill. The name actually gave a hint of what to expect on the new UAV: long range, long endurance, efficient and graceful in the external appearance. The last requirement is obviously not a stringent one but the primary goal of the project is to conduct a cross-sea flight demonstration to an offshore county of Taiwan, the Penghu Islands (see Fig. 1). The direct distance between the selected destination point (a remote islet) and the takeoff point is approximately 44km. This implies that a round trip flight would cover a ground distance of close to 90km. This calls for a new design of an UAV which can fly such a long distance and a more efficient, reliable next generation onboard system.

The outcome of the preliminary design revealed that the airframe was to have a maximum takeoff gross weight of 29·3kg with a 5kg payload capacity, wing span of 4·36m and overall length of 2·73m[11]. It is by far the largest and the heaviest UAV that RMRL has ever attempted to build. Hence, in order to reduce the risk of any uncertainties in building the full-scale aircraft directly, both in terms of cost and time effort, the team decided to build a 60% scaled-down prototype-designated as SP-X.6, which would be used to justify the overall design (see Section 2.1). In particular, the performance and stability characteristics of the prototype would be meticulously assessed for compliance with the design standard. Moreover, the prototype is used in the preliminary efforts in modeling and autopilot design such as those accomplished in the framework of this paper.

2.0 SYSTEM CONFIGURATION

2.1 Air vehicle

The preliminary design of the full-scale Spoonbill UAV was documented in Chan *et al*[11]. The design was tailored to meet the requirements associated with the Spoonbill project where the aircraft



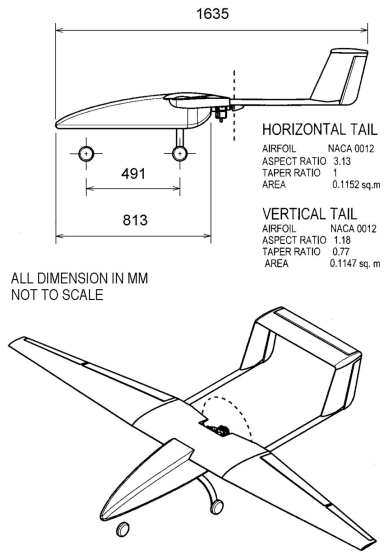


Figure 2. Schematic drawings showing general layout and dimensions of SP-X.6.

https://doi.org/10.1017/S0001924000002955 Published online by Cambridge University Press



Figure 3. SP-X.6.

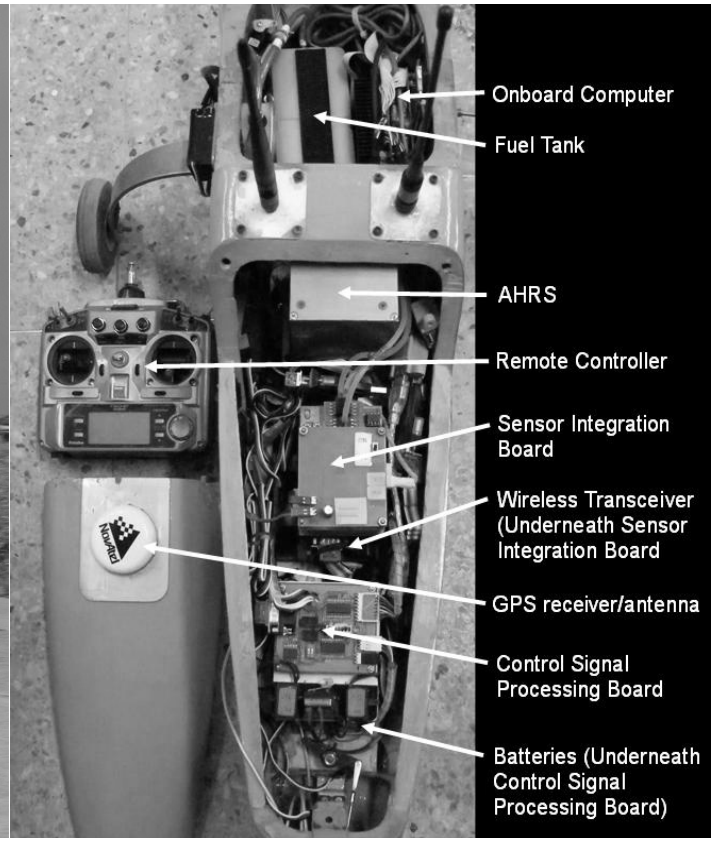


Figure 4. Onboard avionics system.

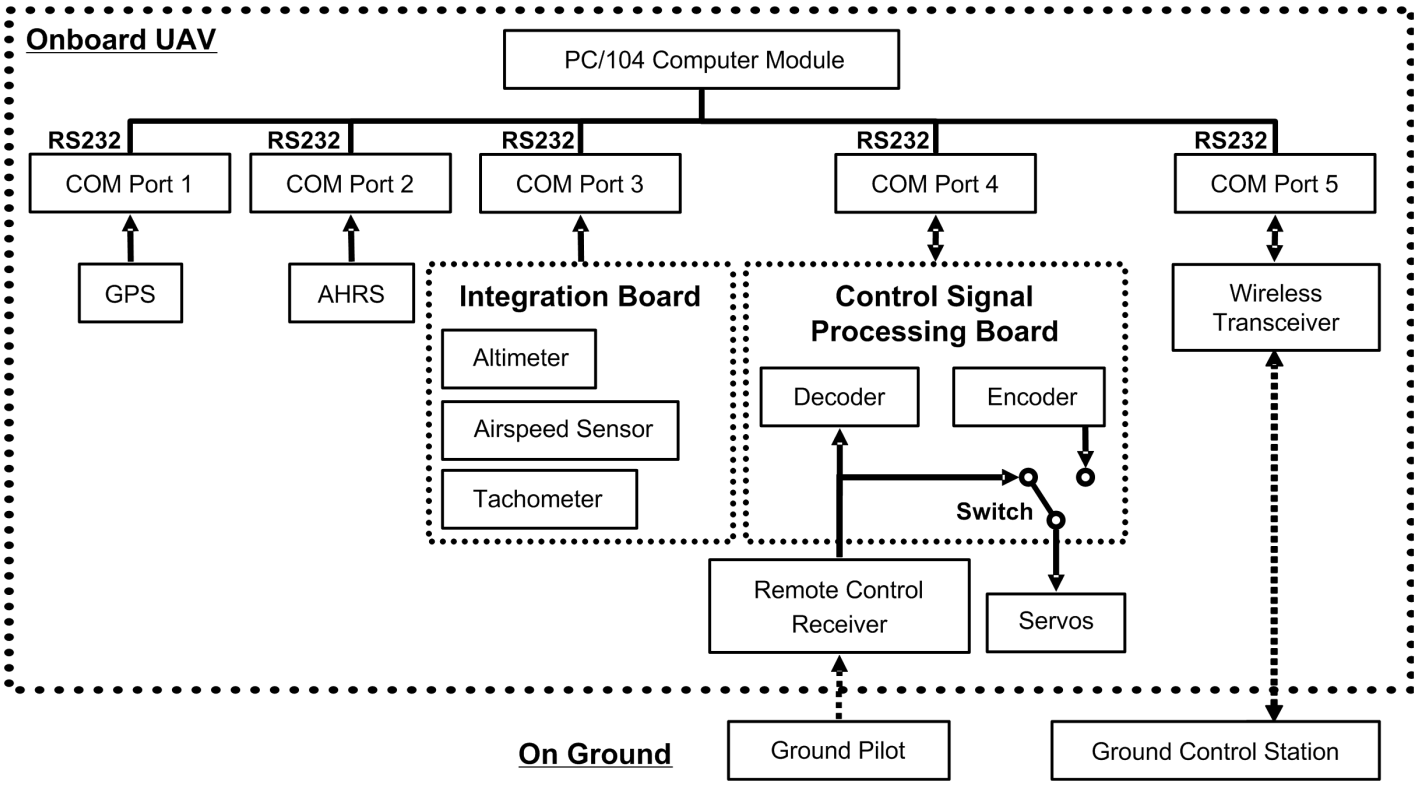


Figure 5. Onboard avionics system architecture of SP-X.6.

https://doi.org/10.1017/S0001924000002955 Published online by Cambridge University Press

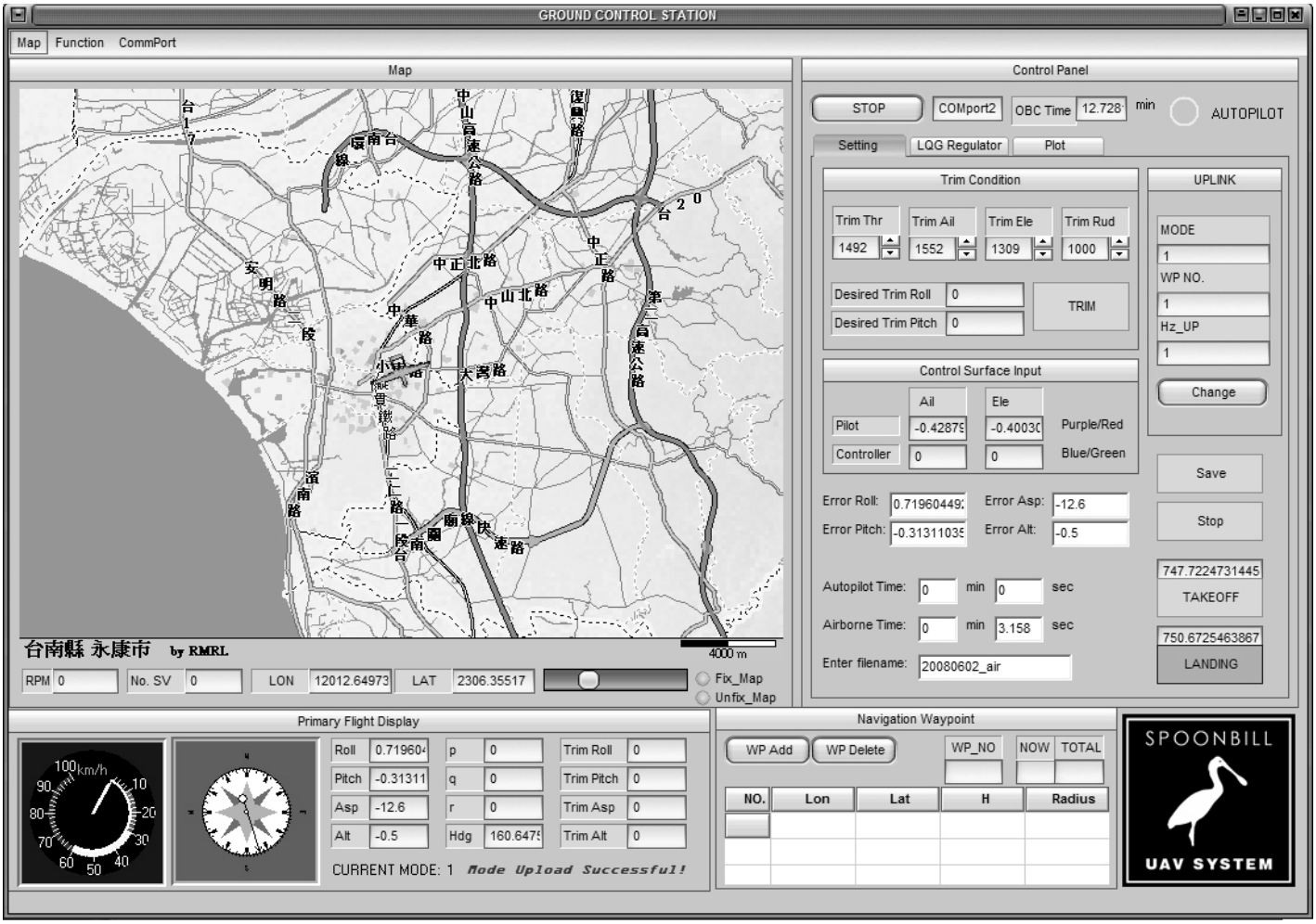


Figure 6. Snapshot of ground control station program user interface.

was to be inherently stable, efficient, capable of sustaining long endurance flight and structurally simple. The actual aircraft used to produce the work described in this paper is a direct 60% scaled prototype, which is designated as SP-X.6. Therefore the design features are essentially identical to the full-scale Spoonbill UAV.

In general, the aircraft is conventionally configured characterised by high-wing, twin-boom and pusher type engine as illustrated in Figs 2 and 3. High-wing configuration assures the lateral/directional stability and simplifies the assemble/disassemble process. Pusher engine installment provides a clean airflow over the wing and fuselage which results in a smaller overall skin drag. At the same time, video/still camera (not shown in Fig. 2) installed at the bottom of the fuselage would have a clearer view.

The SP-X.6 has a wingspan of 2·62m, aspect ratio of 10 and overall length of 1·64m. The maximum take-off gross weight ever registered in previous flight tests was 11·5kg which gives the aircraft a wing loading of 165·2N/m^2. To provide sufficient thrust to lift the aircraft off the ground, a 25·4cc two-stroke gasoline piston engine is installed. As regards the structure, the fuselage is mainly constructed from fiber glass with wooden frame reinforcement while the wing and tailplanes are built from balsa wood. In the mean time, two aluminum-alloy booms connect the tailplanes to the wing.

2.2 Onboard avionics system

The onboard avionics system of the spoonbill UAV system consists of an onboard computer (OBC), an attitude and heading reference system (AHRS), a Global Positioning System (GPS) receiver, air data sensors which include altimeter, airspeed sensor, tachometer, and a wireless transceiver (see Figs 4 and 5). Most of the devices are off-the-shelf products but the data integration and preprocessing, however is done by using integrated electronic circuit boards designed and fabricated by RMRL. The OBC is a PC/104 embedded-PC type computer module capable of running on Windows-based operating system. All peripheral subsystems communicate with the OBC via five communication ports (COM ports) through RS-232 protocols as depicted in Fig. 5. The system architecture shown in Fig. 5 enables the signals from the sensors to be fed into OBC in readily usable digital form. This feature significantly reduces the computational burden of the OBC for it does not have to deal with signal conditioning tasks such as A/D (analogue-to-digital) conversion and thus would be more efficient in executing data acquisition, storage and flight control programs. With the utilisation of microcontrollers, the sensor integration board (see Fig. 4) preprocesses signals captured by air data sensors and tachometer and then concatenates them into a single package of binary code which would be sent to the OBC.

On the other hand, the control signals provided by the pilot in the form of pulse-width modulation (PWM) signals are captured and decoded using microcontroller as well. This is done in the control signal processing board shown in Fig. 5. Note that there is a switch governing the control signals delivered to the servos of the aircraft's control surfaces. When the pilot engages the autopilot, the switch would cut off PWM signals from the pilot and allow the aircraft to be fully controlled by the OBC. The encoder basically converts the

https://doi.org/10.1017/S0001924000002955 Published online by Cambridge University Press

amount of required control inputs computed by the flight control algorithm in OBC into corresponding PWM signals. All data acquisition and flight control algorithms are executed at a rate of 10Hz. Concurrently, 33 selected flight parameters are recorded into a CF (compact flash) memory card for post-flight analysis, at the same sampling rate as well.

2.3 Ground control station

When the aircraft is airborne, there must be some means for the operating personnel who remain on the ground to monitor the health status and current location of the aircraft. This is accomplished by using a pair of radio transceivers, each installed in the airborne aircraft and at the ground control station (GCS) respectively. As long as the data acquisition and flight control program is executing normally, the OBC will continuously transmit selected flight data to the GCS at a rate of 2Hz. By using a graphical user interface program, such as the one shown in Fig. 6, those flight data are displayed at the GCS for easy reference. Figure 6 also shows an icon indicating the aircraft location with respect to a local electronic map which is translated from the real-time GPS position data.

Besides monitoring aircraft's flight condition, it is also possible to upload some desired commands to the OBC through the GCS. This function is especially important at the development stage of the autopilot system where a lot of system tests are carried out. For instance, various modes of controllers may be changed in-flight to test their effectiveness in a single flight sortie. Some desired flight variables such as altitude, airspeed, trimmed condition settings and aircraft destination waypoints can also be uploaded to the airborne OBC without having the need to land the aircraft. A well-designed GCS program may improve the efficiency of a flight test program markedly and thus prevent the waste of unnecessary time, labor and cost.

3.0 AIRCRAFT MODELING AND IDENTIFICATION

3.1 Aircraft linearised models

In order to design stability augmentation autopilot using linear-quadratic-Gaussian (LQG) approach, the importance of accurate mathematical models which describe the aircraft dynamics cannot be overemphasised. First, it is assumed that the aircraft dynamics may be decoupled into longitudinal motion and lateral motion, which is a legitimate assumption for conventionally configured aircraft. Next, by applying further simplifications, small perturbation theory, and Taylor's series expansion, the complete six degree-of-freedom nonlinear aircraft equations of motion can be linearised about the trim condition into the following state-space equations:

For longitudinal motion,

$$\begin{bmatrix} \Delta\dot{V} \\ \Delta\dot{\alpha} \\ \Delta\dot{q} \\ \Delta\dot{\theta} \\ \Delta\dot{h} \end{bmatrix} = \begin{bmatrix} X_V & \frac{X_\alpha}{V_0} & 0 & -g\mathrm{Cos}\theta_0 & 0 \\ \frac{Z_V}{V_0} & \frac{Z_\alpha}{V_0} & 1+\frac{Z_q}{V_0} & g\mathrm{Sin}\theta_0 & 0 \\ M_V+\frac{Z_V M_{\dot\alpha}}{V_0} & M_\alpha+\frac{Z_\alpha M_{\dot\alpha}}{V_0} & \left(1+\frac{Z_q}{V_0}\right)M_{\dot\alpha}+M_q & \frac{-g\mathrm{Sin}\theta_0 M_{\dot\alpha}}{V_0} & 0 \\ 0 & 0 & 1 & 0 & 0 \\ 0 & -V_0 & 0 & V_0 & 0 \end{bmatrix} \begin{bmatrix} \Delta V \\ \Delta\alpha \\ \Delta q \\ \Delta\theta \\ \Delta h \end{bmatrix} + \begin{bmatrix} X_{\delta_e} \\ \frac{Z_{\delta_e}}{V_0} \\ M_{\delta_e}+\frac{Z_{\delta_e}M_\alpha}{V_0} \\ 0 \\ 0 \end{bmatrix} \Delta\delta_e \quad \ldots (1)$$

For lateral motion,

$$\begin{bmatrix} \Delta\dot{\beta} \\ \Delta\dot{p} \\ \Delta\dot{r} \\ \Delta\dot{\phi} \end{bmatrix} = \begin{bmatrix} \frac{Y_\beta}{V_0} & \frac{Y_p}{V_0} & -\left(1-\frac{Y_r}{V_0}\right) & \frac{g\mathrm{Cos}\theta_0}{V_0} \\ L_\beta & L_p & L_r & 0 \\ N_\beta & N_p & N_r & 0 \\ 0 & 1 & 0 & 0 \end{bmatrix} \begin{bmatrix} \Delta\beta \\ \Delta p \\ \Delta r \\ \Delta\phi \end{bmatrix} + \begin{bmatrix} 0 & Y_{\delta_r} \\ L_{\delta_a} & L_{\delta_r} \\ N_{\delta_a} & N_{\delta_r} \\ 0 & 0 \end{bmatrix} \begin{bmatrix} \Delta\delta_a \\ \Delta\delta_r \end{bmatrix} \quad \ldots (2)$$

Note that the state vectors consist of total velocity, V, altitude, h, angular velocity components, $\{p, q, r\}$, pitch and bank angles, $\{\theta,\phi\}$, angle-of-attack and sideslip angle, $\{\alpha,\beta\}$. There are three control inputs, namely deflections of elevator, δ_e, ailerons, δ_a, and rudders, δ_r. Meanwhile, the system matrices are made of unknown parameters which are basically constant with respect to a specific equilibrium (trim) condition. They consists of various derivatives of the applied aerodynamic force components, $\{X, Y, Z\}$ and the applied aerodynamic moment components, $\{L, M, N\}$, all acting on the aircraft body-axis coordinate frame. Note that V_0 and θ_0 denote trim airspeed and trim pitch angle respectively. The definitions of the associated variables are illustrated in Fig. 7 and the complete derivation of Equation (1) and Equation (2) may be found in Lee[14]. The 'Δ' denotes that the variables are perturbations from the trimmed conditions.

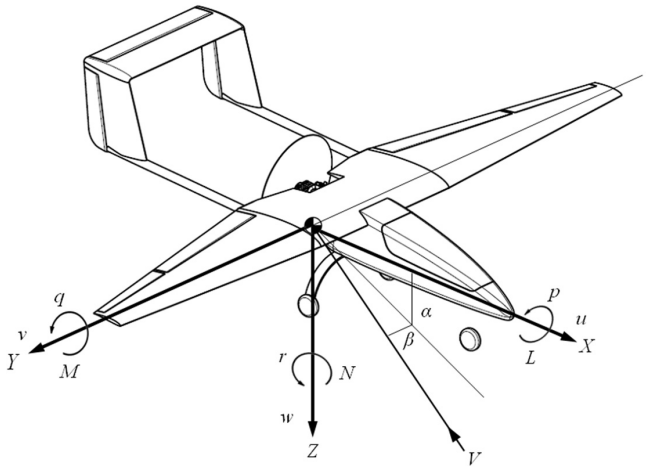


Figure 7. Definition of variables on the aircraft body-axis frame.

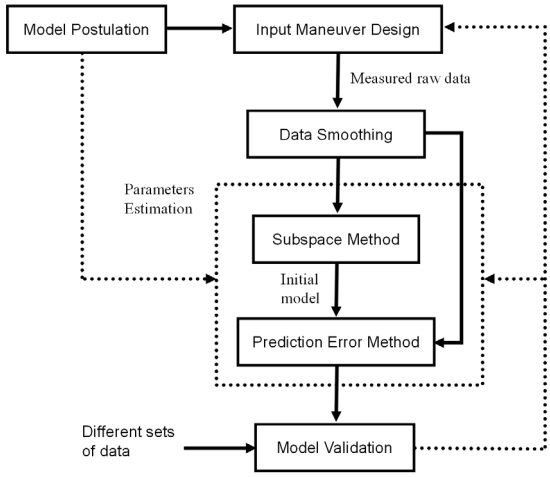


Figure 8. Flow diagram of system identification routine.

https://doi.org/10.1017/S0001924000002955 Published online by Cambridge University Press

3.2 System identification

The previous section showed that the linearised aircraft dynamics may be structured and expressed in the form of linear state-space equation. The equivalent state-space equations in discrete time domain are:

$$\mathbf{x}(k+1) = \mathbf{A}\mathbf{x}(k) + \mathbf{B}\mathbf{u}(k) + \mathbf{H}\mathbf{w}(k)$$
$$\mathbf{y}(k) = \mathbf{C}\mathbf{x}(k) + \mathbf{v}(k) \quad \ldots (3)$$

where k is the number of time-step. Note that **x**, **u**, **y**, **w** and **v** are the system state, control input, measured output, process noise and measurement noise vectors respectively. The remaining **A**, **B**, **C** and **H** are the so-called system matrices which determine the dynamics of the aircraft motion and they are known to be constant with respect to a particular equilibrium (trimmed) flight condition.

In general, the unknown parameters in the system matrices, **A**, **B**, **C** and **H** can be obtained via wind-tunnel testing or computational fluid dynamics (CFD) computation. However, wind-tunnel testing is time-consuming, laborious and costly which may not yield accurate results if the tests were not done in sufficiently meticulous way. On the other hand, CFD computation is equally time-consuming and the results depend heavily on the quality of the CFD algorithm. That requires a large research and computational effort, not to mentioned the cost incurred thereof. As an alternative, the problem can be recast as a system identification problem which may then be solved by using a variety of available system identification tools which require only the input and output data, i.e. **u** and **y**. In particular, two well established identification methods, namely the subspace identification method and the prediction error method (PEM) are selected to determine the longitudinal and lateral models of the Spoonbill UAV. In this paper, the authors propose using a combination of subspace and PEM identification for both identification methods complement each other in an effective way. The subspace method has the merit of being simple and efficient while providing a good level of model accuracy which compliment well with the recursive PEM method. The latter is an optimisation algorithm that requires a good initial model to prevent the optimisation solution from falling into local minima.

Figure 8 elucidates the simple and straight forward procedures of aircraft system identification routine proposed by the authors. First, raw flight data are collected from specific flight manoeuvres designed by taking into account the model structure and the inherent characteristics of the system dynamics. The design of input forms for flight manoeuvres is important because the input manoeuvre design influences the aircraft response, which in turn affects the dynamic content in the sampled data. In essence, the objective of input manoeuvre design is to excite the dynamic system so that the data contain sufficient information for accurate modeling, subject to the practical constraints of the experiments. This translates into exciting the dynamic response modes such that the sensitivities of the model outputs to parameters are high and correlations among the parameters are low. The difficulty in designing input manoeuvre for UAV is that, the input amplitude needs to be large enough to excite natural dynamics modes of the aircraft without sacrificing flight safety. On the other hand, the aircraft response must be limited to perturbations about the equilibrium flight condition, in order to retain the validity of the local model structure such as those developed in Section 3.1. Furthermore, the output perturbations must also be bounded so that the small perturbation requirement necessary for decoupling longitudinal and lateral dynamic equations is satisfied. The type of input manoeuvre forms selected for the Spoonbill system identification are the multi-steps inputs shown in the Fig. 9 and Fig. 10, as suggested in Klein and Morelli[15]. They are chosen due to the rich frequency spectrum covered in the input excitation which would result in better quality of dynamic response data.

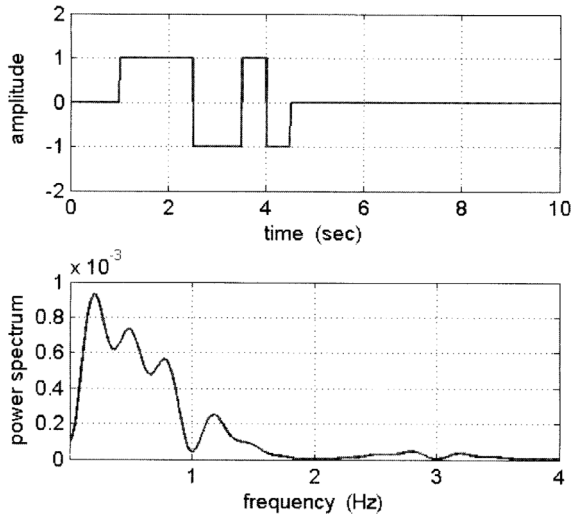


Figure 9. Multi-steps input applied on longitudinal identification manoeuvres[15].

Since the raw data are usually contaminated by environmental noises and random errors, data filtering or smoothing is performed to improve the quality of the identification data. In particular, a type of global Fourier smoothing with an optimal Wiener filter developed by Morelli[16] is implemented. Then, an initial model is obtained by using subspace identification method. By feeding the initial model into an iterative prediction error minimisation algorithm, a set of refined model parameters are attained. The last and crucial step in the system identification process is validation of the model. The identified model must demonstrate that it has good prediction capability on comparable manoeuvres. This is accomplished by testing the prediction capability of the model on data that is not used in the identification process. The measured input for the prediction data is applied to the identified model to generate predicted responses, which are then compared with measured values.

3.3 Identification methods

The subspace identification method has been a well accepted method for identification of multivariable linear system. The key point in subspace identification is the reconstruction of the state sequence or the so-called Kalman state sequence directly from input-output data without knowing the model[17]. This can be done via orthogonal or

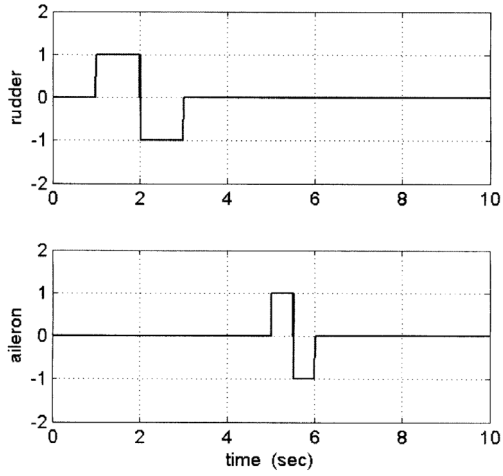


Figure 10. Multi-steps inputs applied on lateral identification manoeuvres[15].

https://doi.org/10.1017/S0001924000002955 Published online by Cambridge University Press

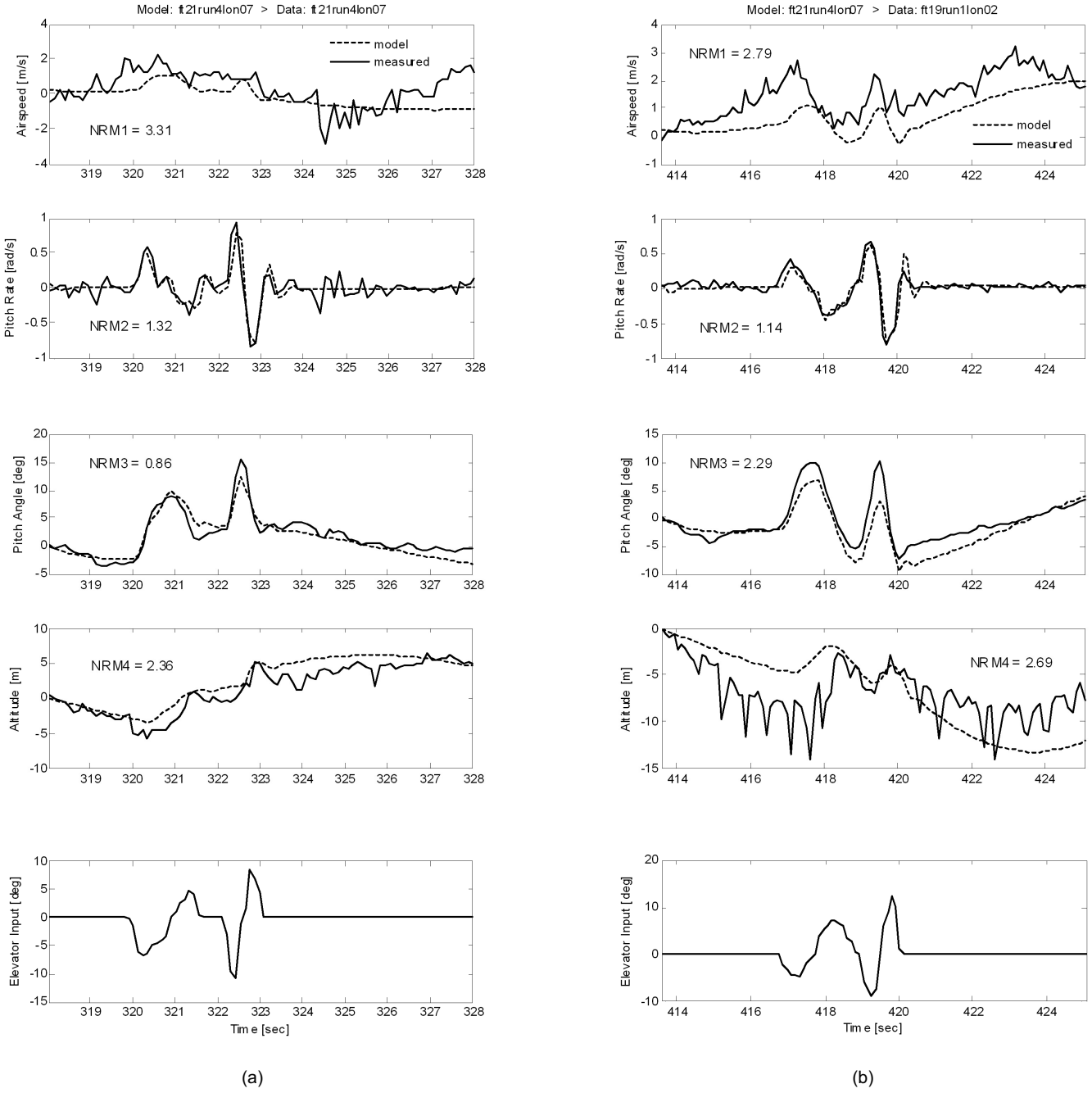


Figure 11. Longitudinal identification results: Comparison with (a) identification data; (b) verification data.

oblique projection and singular value decomposition. Once an estimate of the state sequence is available, the unknown system matrices, $\boldsymbol{A}$, $\boldsymbol{B}$, $\boldsymbol{C}$ and $\boldsymbol{H}$ are obtained by solving two least squares problems based on Equation (3).

In the mean time, prediction error method is a classical identification method which typically refers to a class of identification algorithms designed so that a function of prediction errors is minimised. It is a recursive optimisation method which requires a good initial guess of the model for there is a risk of falling into local minima in the process of minimising the prediction errors. Hence, subspace method is first used to obtain a good initial model which would be fed into the PEM algorithm resulting in an optimised and refined model.

The major advantage of this identification scheme is that it is simple, straight forward and efficient. On top of that, the algorithms for the subspace and PEM computation are readily available in the MATLAB®/System Identification Toolbox™. In particular, the commands 'n4sid' and 'pem' are utilised, which corresponds to subspace and prediction error method respectively. In the mean time, the data smoothing and model validation algorithms are also written in MATLAB® programming environment. Provided the required identification data, the resultant model can be obtained in the matter of seconds. This means that a large amount of data sets can be processed and evaluate in reasonably short time. In addition, to make the scheme more attractive, this aircraft identification routine is readily applicable to any other UAV system as long as the associated air vehicle is of fixed wing, conventional configuration.

https://doi.org/10.1017/S0001924000002955 Published online by Cambridge University Press

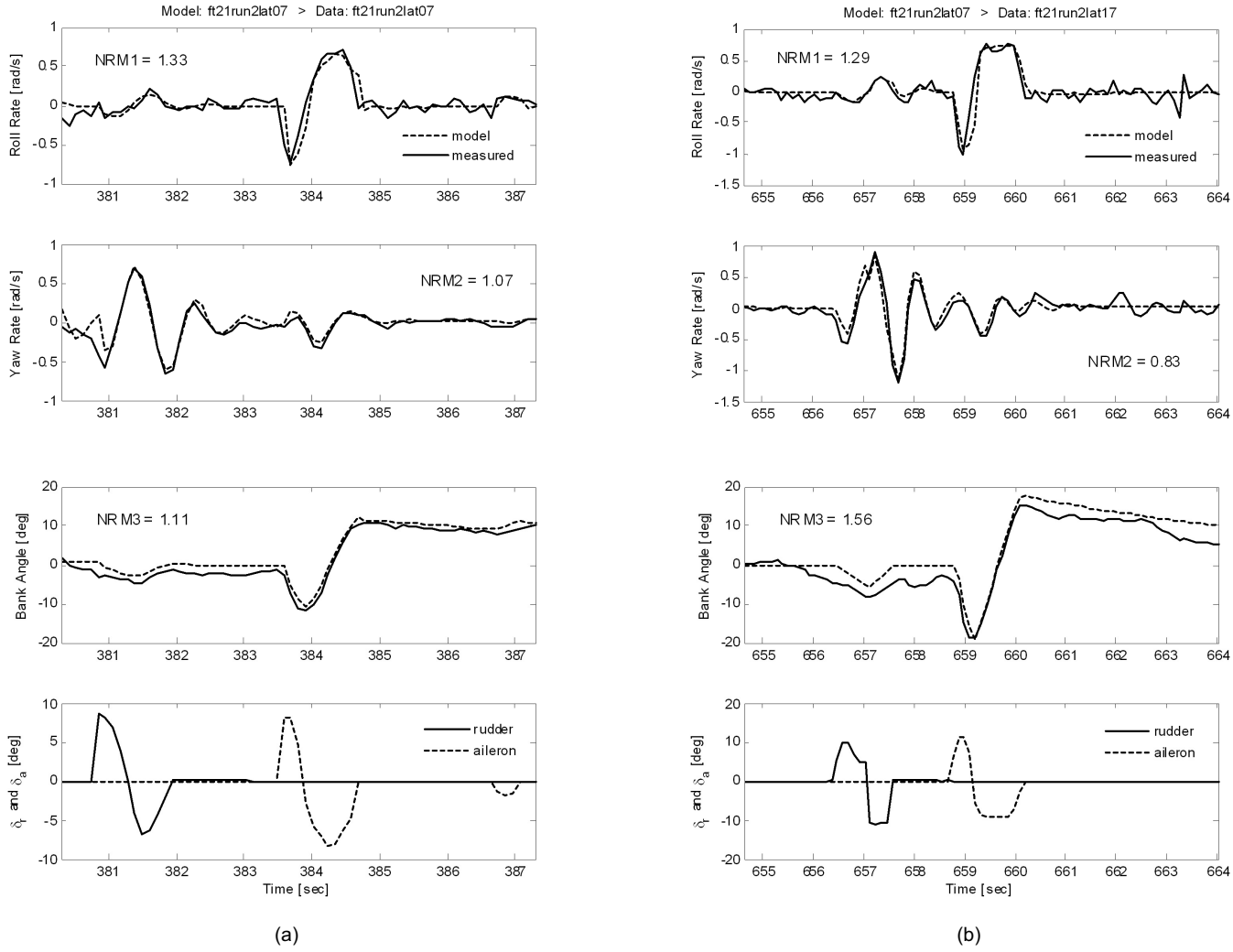


Figure 12. Lateral identification results: Comparison with (a) identification data; (b) verification data.

3.4 Identification results

A series of flight tests were conducted using the UAV system described in Section 2 which spanned three different days in April of 2008 to collect the input-output data required for system identification. Input manoeuvres depicted in Fig. 9 and Fig. 10 were performed separately for longitudinal and lateral motion as soon as the aircraft was brought into a trimmed, straight and level flight condition. However, since all flight manoeuvres were performed manually by a ground pilot using remote controller, it is practically impossible for the pilot to repeat the exact same trim condition for all input manoeuvre runs. The only parameter that the pilot is able to maintain constant throughout flight manoeuvres is the throttle level which corresponds to the engine speed. Therefore, for each input manoeuvre run, the flight condition at the beginning of manoeuvre is taken as the trim condition for that particular run. In that regards, collected data sets would be checked in post-flight analysis to ensure that the trim conditions were within acceptable range.

By using the identification routine highlighted in Fig. 8, a total of 106 eligible data sets (69 of longitudinal and 37 of lateral) were collected and this yielded 106 identified models. Hence, it is necessary to have some sort of performance index to evaluate the quality of the identified models. In that regards, the authors propose using the norm, NRM. Essentially, the identified model's predicted output response, $\hat{y}$ is compared with the corresponding measured output data, y. Let the difference between predicted output and the measured output be ξ and it is given by;

$$\xi_i = \frac{\hat{y}_i - y_i}{y_i} \qquad i = 1,2,3,...N \qquad \ldots (4)$$

Note that i is the sequence of data and N is the total number of data. The norm of a vector presents a measure of 'length' of the vector. Hence the norm of ξ gives a sense of 'size' of the difference between y and $\hat{y}$ and it is computed as

$$\text{NRM} = \|\xi_i\| = \left(\frac{\hat{y}_i - y_i}{y_i}\right)^T \left(\frac{\hat{y}_i - y_i}{y_i}\right) \qquad i = 1,2,3,...N \qquad \ldots (5)$$

or in practice, the authors computes the norm via MATLAB® command 'norm'. Note that NRM ≥ 0 and a perfect fit (between y and $\hat{y}$) corresponds to NRM = 0. In other words, the smaller the value of NRM, the better the quality of the identified model. Analysis showed that acceptable fits are typically characterised by a norm of less than three.

Using norm, NRM as the performance index, we have arrived at two final models which correspond to aircraft longitudinal and lateral dynamics respectively. The associated identification results are presented in Figs 11 and 12. Figure 11(a) shows that in general, the agreement between the predicted responses from the model and the actual responses is good. This is substantiated by the low values of

https://doi.org/10.1017/S0001924000002955 Published online by Cambridge University Press

norm of each output which is typically less than three with the exception of the airspeed response. Furthermore, it is observed that the fits in pitch rate and pitch angle responses are better with norms of 1·32 and 0·86 correspondingly. Relatively poorer fits for airspeed and altitude responses are reflected in the norms of 3·31 and 2·36. In the mean time, in order to challenge the fidelity of the model, it is then tested with another set of flight data associated with similar input manoeuvre (verification data). The comparison results are shown in Fig. 11(b) where the model is found to be capable of predicting the response outputs quite well even though the data were not used to identify the model in the first place. The corresponding norms also indicate that the quality of the fits is encouragingly high. It is noteworthy that the input manoeuvres (elevator deflection) applied during the flight is the one shown in Fig. 9 where by convention a negative input would induce a pitch-up (nose-up) motion on the aircraft, and vice-versa. The distortion on the input form is introduced by the pilot because it is impossible for the pilot to manually apply the same input form as in Fig. 9 precisely. Nevertheless, the results showed that the distortions did not impose significant adverse effects on the identified model.

On the other hand, the case for the lateral model follows similar argument to the discussion on longitudinal model previously. Figure 12 shows that the performance of the lateral model is very good indeed. This is evident in the very low values of norm observed for all output responses with magnitude of practically less than two. The same good agreement is observed for the case when the model was tested with verification data, as vividly shown in Fig. 12(b). Overall, the lateral model slightly outperforms the longitudinal model. The reason is believed to stem on the fact that there are two air data included in the output vector of the longitudinal model. Air data are known to be corrupted with environmental and signal noises which inevitably impose damaging effects on the identification algorithm. The lateral model however, contains only attitude data in the output vector. Attitude data are provided by the AHRS which has significantly lower noise than the air data sensors.

Since the exact model of the newly designed Spoonbill UAV is not available, it is difficult to precisely verify the accuracy of the model presented. Nevertheless, it is well understood that the best way to test the outcome of the system modeling identification is to implement the controller based on the identified model. In contrast to the mathematicians, in the control engineer's point of view, the 'accuracy' of a model is not determined by how much it deviates from the 'true' model, but the performance of the controller design upon that model. As long as the controller meets the design specification, the modeling effort is considered as a successful one.

4.0 AUTOPILOT DESIGN AND SIMULATION

4.1 Linear-quadratic-Gaussian regulator

With the longitudinal and lateral models at hand, we may proceed to design the autopilot for Spoonbill UAV. The linear-quadratic-Gaussian (LQG) design approach is chosen due to its well-established theoretical and mathematical background, as well as the simplicity in the design procedures and the resultant control law. Essentially, LQG regulator is the combination of the linear-quadratic regulator (LQR) and the Kalman filter. The authors believe that LQR and Kalman filter need no elaborate introduction for they have been widely used in various disciplines of control engineering. In short, recall that for a system expressed in the linear state-space form as Equation (3), LQR approach assumes a full state feedback control law:

$$\mathbf{u}(k) = -\mathbf{K}\mathbf{x}(k) \quad \ldots (6)$$

where the optimal feedback gain, $\mathbf{K}$ is obtained such that the quadratic cost function, J.

$$J = \sum_{k=1}^{\infty} \left[\mathbf{x}(k)^T \mathbf{Q}\mathbf{x}(k) + \mathbf{u}(k)^T \mathbf{R}\mathbf{u}(k) \right] \quad \ldots (7)$$

is minimised. Note that $\mathbf{Q}$ and $\mathbf{R}$ are the symmetric positive semi-definite weighting matrices which determine the accuracy of the controller and the amount of control effort required, respectively.

On the other hand, the Kalman filter is an efficient recursive filter that estimates the state of a dynamic system from a sequence of noisy measurements. Assuming that the process noise, $\mathbf{w}$ and measurement (sensor) noise, $\mathbf{v}$ are zero mean white noises with variance of $\mathbf{Q}_k$ and $\mathbf{R}_k$ respectively, the resulting optimal observer has the dynamics described by[18].

$$\hat{\mathbf{x}}(k+1 \mid k) = \mathbf{A}\hat{\mathbf{x}}(k \mid k-1) + \mathbf{B}\mathbf{u}(k) + \mathbf{L}\left[\mathbf{y}(k) - \mathbf{C}\hat{\mathbf{x}}(k \mid k-1)\right] \quad \ldots (8)$$

where $\hat{\mathbf{x}}$ is the estimated states and $\mathbf{L}$ is the estimator gain.

Full state feedback LQR is attractive because the closed-loop system is guaranteed to be stable[18]. In addition, it also has certain guaranteed robustness properties that make it even more suitable for application on flight controls. However, full state measurement is rarely available in practice. In fact, this is exactly the case for Spoonbill UAV system where the angle-of-attack, α and the sideslip angle, β are not measured. A way to surpass this inadequacy is to incorporate an observer, for instance Kalman filter into the controller to estimate the system states using the available output, $\mathbf{y}$ and known control input, $\mathbf{u}$. Now, instead of using the actual states, $\mathbf{x}$, the estimated states, $\hat{\boldsymbol{x}}$ is fed back to form the control law:

$$\mathbf{u}(k) = -\mathbf{K}\hat{\mathbf{x}}(k) \quad \ldots (9)$$

The concatenation of LQR and Kalman filter forms the LQG regulator shown in Fig. 13. When applied to an aircraft, it is basically a stability augmentation autopilot where the aircraft is maintained at specific equilibrium (trim) conditions where the states, $\mathbf{x}$ and output, $\mathbf{y}$ are regulated to zero.

4.2 Autopilot design procedures

Two independent LQG controllers constitute the autopilot of the Spoonbill UAV system which governs the control of longitudinal and lateral motions of the aircraft concurrently. Essentially, the LQG regulator regulates the states of the system to zero. Due to the robustness nature, the autopilot would also be able to reject random or environmental disturbances encountered during flight.

The flow diagram showing the entire iterative design procedure is depicted in Fig. 14 where the design procedure starts with the selection of the weighting matrix, $\mathbf{Q}$, $\mathbf{R}$ for the LQR and $\mathbf{Q}_k$, $\mathbf{R}_k$ for the Kalman filter. Then, together with the state-space model of the

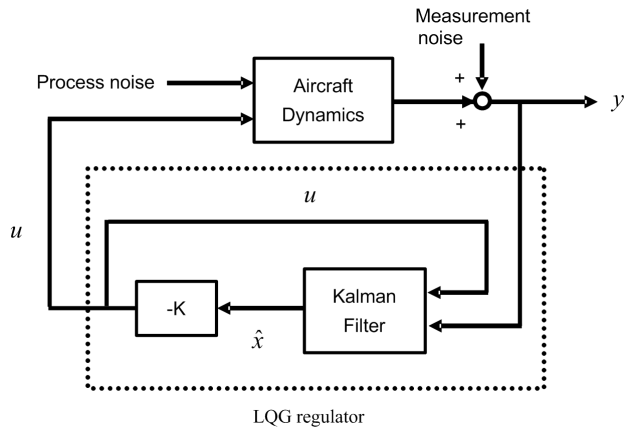


Figure 13. LQG regulator.

https://doi.org/10.1017/S0001924000002955 Published online by Cambridge University Press

aircraft identified in Section 3, the optimal gain, **K** of LQR and estimator gain, **L** of Kalman filter are obtained by using MATLAB® command 'dlqr' and 'kalman' respectively. After that, by using another MATLAB® command 'lqgreg', the LQG regulator is generated by connecting Kalman filter to the LQR. It is noteworthy that the resulting LQG regulator is given in discrete-time state-space equation with a control rate of 10Hz.

In order to check the performance of the LQG regulator, computer simulations are subsequently done using MATLAB®/Simulink software or any other types of suitable computer program. An arbitrary initial condition is given to the controlled system where the time response is observed and analyzed. If the response characteristic such as stability characteristics, overshoot, settling time, etc were satisfactory, the autopilot would be further verified by conducting actual flight test. If not, the process returns to the selection of weighting matrices. The weighting matrices are tuned until the autopilot produces an acceptable time response to an initial perturbation of system state.

Selection of Weighting Matrices, **Q**, **R**, $\mathbf{Q_k}$, $\mathbf{R_k}$

Recall that **Q** and **R** are the weighting matrices for LQR and $\mathbf{Q_k}$ and $\mathbf{R_k}$ are the weighting matrices for Kalman filter (see Section 4.1). A convenient guideline for selecting Q and R is proposed by Bryson and Ho[19]. Suppose we define a performance output,

$$\mathbf{z} = \mathbf{W}\mathbf{x}$$

so that **W** is given and consider the following cost function to be minimised

$$J = \sum_{k=1}^{\infty}\left[\mathbf{z}(k)^T\,\overline{\mathbf{Q}}\mathbf{z}(k) + \mathbf{u}(k)^T\mathbf{R}\mathbf{u}(k)\right]$$

This implies that only a subset of **x**, i.e. **z** would be regulated to zero. Comparing with Equation (7) yields

$$\mathbf{Q} = \mathbf{W}^T\overline{\mathbf{Q}}\mathbf{W}$$

According to Bryson and Ho[19], $\overline{\mathbf{Q}}$ and **R** may be chosen using the maximum allowable deviations in $\mathbf{z}(k)$ and $\mathbf{u}(k)$. Now, define the maximum allowable deviation in component $\mathbf{z}_i(k)$ of $\mathbf{z}(k)$ as z_{iM} and the maximum allowable deviation in component $u_i(k)$ of the control input $\mathbf{u}(k)$ as u_{iM}. Then $\overline{\mathbf{Q}}$ and **R** may be selected as $\overline{\mathrm{Q}} = \mathrm{diag}\{q_i\}$, with $\mathrm{R} = \mathrm{diag}\{r_i\}$, with;

$$q_i = \frac{1}{z_{iM}^2} \qquad r_i = \frac{1}{u_{iM}^2}$$

The rationale behind the choice is pointed out appropriately by Stevens and Lewis[18]. For instance, as the allowed limits z_{iM} on $z_i(k)$ decreases, the weighting in the cost function placed on $z_i(k)$ increases, which requires smaller excursions in $z_i(k)$ in the close-loop system.

On the other hand, the selection of $\mathbf{Q_k}$ and $\mathbf{R_k}$ is relatively easy where they represent the covariance of process noise and measurement noise respectively. The corresponding covariance values may be estimated from actual flight test measurements or simply by trial-and-error experience. Since the entire design procedure is simple and efficient, thanks to readily available commercial algorithm packages, repeated trials and tuning of weighting matrices may be achieved in relatively small amount of time, typically in the order of tens of minutes. For detail synthesis of the longitudinal and lateral LQG regulators using the procedures depicted in Fig. 14, readers are referred to Lee[14] for detail elaboration.

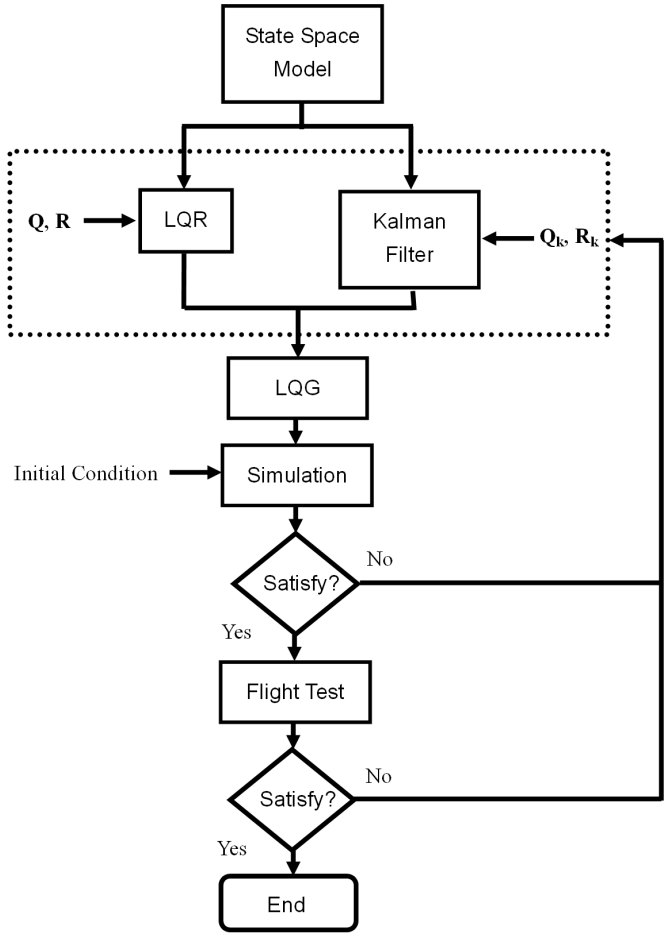


Figure 14. Flow chart showing LQG autopilot design procedures.

4.3 Simulation results

Following the procedures outlined in the previous section, longitudinal and lateral LQG controllers were constructed by selecting the values of the weighting matrices **Q**, **R**, $\mathbf{Q_k}$, $\mathbf{R_k}$. Subsequently, computer simulations were immediately performed after the controllers were generated by the algorithm. Judging from the simulation results, the weighting matrices were repeatedly tuned until desired system time responses were obtained. Figure 15 shows the simulation results of three longitudinal controllers corresponding to three different choices of weighting function as listed in Table 1. Note that for the longitudinal motion, there is only one performance output, i.e. the altitude associated with one command input, the elevator deflection.

Table 1
Selection of elements of weighting matrices (Longitudinal)

Controller Designation	z_M [m]	u_M [rad]
Lon#1	10	10π/180
Lon#2	5	8π/180
Lon#3	12·5	8π/180

The stability of the closed-loop longitudinal dynamics is vividly shown where all states settled to zero (trim values) within six seconds for all three controllers (see Fig. 15). In addition, all responses show favorable transient behaviors where only acceptably small overshoot are observed. The control effort, i.e. the elevator deflection input is also within acceptable margin. This is achieved by tuning the value of

https://doi.org/10.1017/S0001924000002955 Published online by Cambridge University Press

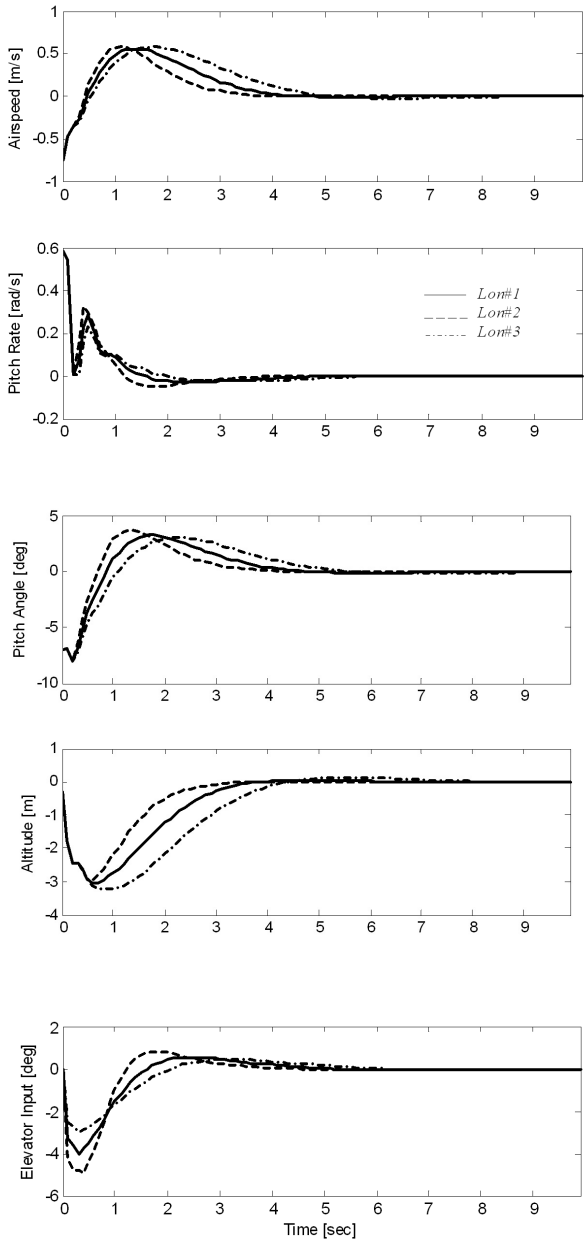


Figure 15. Simulated time response of longitudinal controller subject to initial state perturbation.

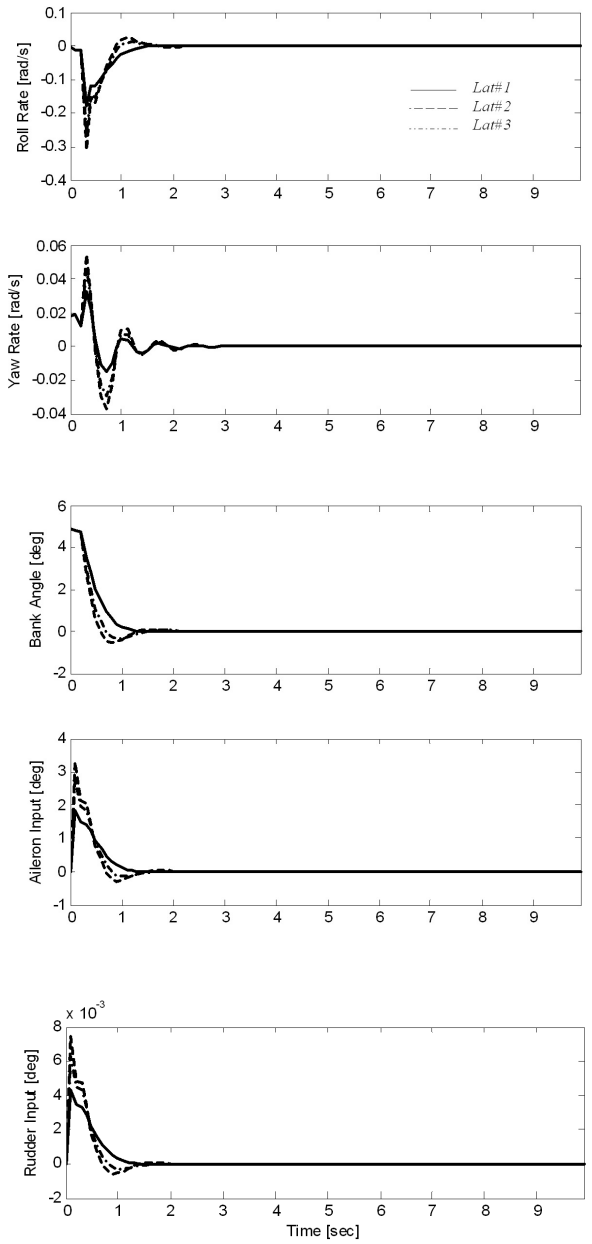


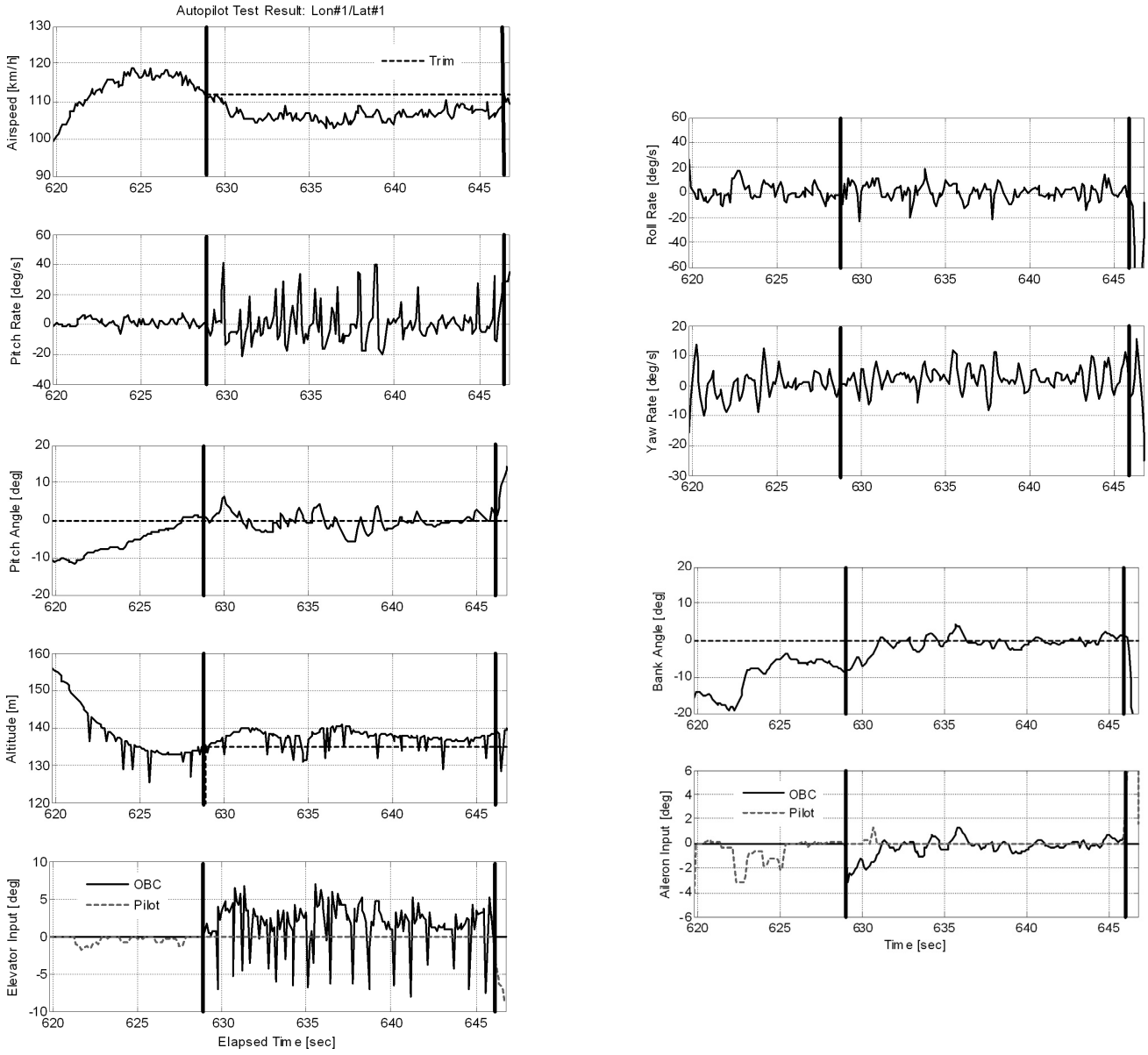
Figure 16. Simulated time response of lateral controller subject to initial state perturbation.

u_M (see Table 1). Among the three controllers, i.e. *Lon#1*, *Lon#2*, and *Lon#3*, it seems that *Lon#2* has the best performance in terms of overshoot and settling time of the performance output, altitude. However, the amount of control input is also larger than the rest. Here, the trade-off between the desired performance and the amount of required control input is clearly exhibited. This is one of the important characteristics of LQG controllers.

Similar arguments may be applied to the lateral dynamics simulation result which is shown in Fig. 16. Again, three lateral controllers were constructed associated with different weighting matrices. Note that the performance output is the bank angle, ϕ while there are two command inputs for lateral control, namely aileron and rudder deflection (see Table 2). The lateral system states converged to steady state in less than 3 seconds with favorable transient properties as well. In particular, controller *Lat#1* performs the best with no overshoot in the bank angle regulation. Moreover, the value of u_{2M} was selected such that the rudder control would be minimal. Figure 16 depicts and proves that the required rudder input for lateral control is indeed negligible. This justifies that it is highly feasible to control the lateral motion of the aircraft solely by ailerons inputs. In fact, due to the hardware limitation in the onboard system, and also for the simplicity of the control laws, only two channels of control inputs, i.e. the elevator and ailerons are used to perform automatic flight of the Spoonbill UAV.

One of the most attractive features of the proposed LQG design approach is that the optimal feedback gains are automatically generated in the design algorithm. No manual tuning is needed on the overall control gains which the work is widely recognised to be a frustrating and time-consuming. The design parameters are the weighting matrices, $\mathbf{Q}$, $\mathbf{R}$, $\mathbf{Q_k}$, $\mathbf{R_k}$, where convenient guidelines may be followed. Furthermore, the guidelines are intuitively linked to the physical variables and their effects on the system. This way, it is a lot easier for the designer to make decision based on desired control effects rather than trial-and-error instinct.

https://doi.org/10.1017/S0001924000002955 Published online by Cambridge University Press



(a) (b)

Figure 17. Flight test results of controllers *Lon#1/Lat#1*. a) Longitudinal; b) Lateral.

Table 2
Selection of elements of weighting matrices (Lateral)

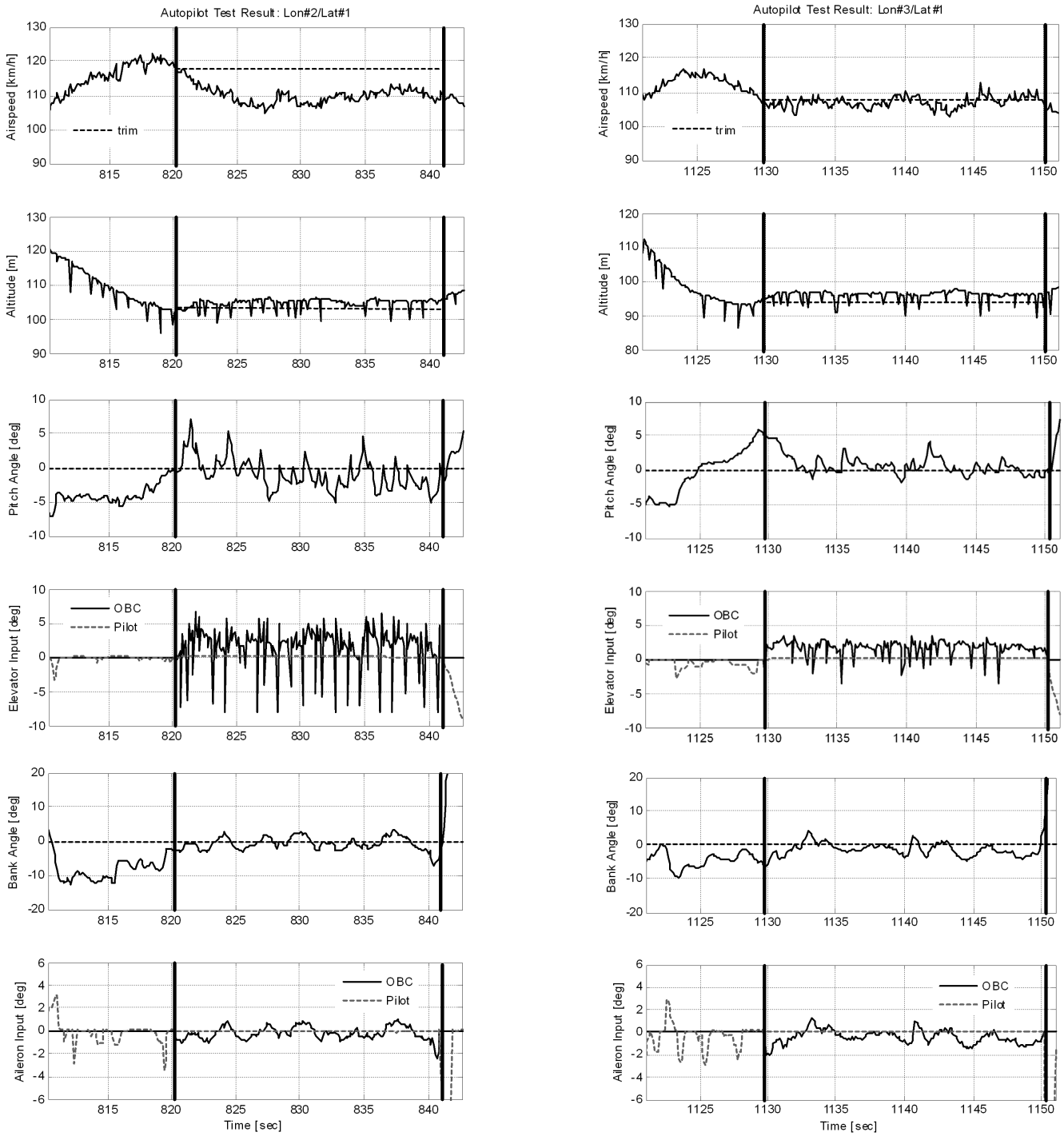
Controller Designation	z_M [rad]	u_{1M} [rad]	u_{2M} [rad]
Lat#1	10π/180	5π/180	0·5π/180
Lat#2	5π/180	5π/180	0·5π/180
Lat#3	10π/180	8π/180	0·8π/180

5.0 FLIGHT TEST RESULTS

Up to this point, we have successfully designed a stability augmentation autopilot for the Spoonbill UAV system by using the techniques and procedures outlined in previous sections. The design process is not complete until the autopilot is put through the ultimate validation in actual flight tests. Series of successful flight tests were conducted at an open area along the riverside of the Zengwun River, located in the southern part of Taiwan. Typically, the aircraft would take off manually under pilot control and reach nominal altitude ranging from 100m to 150m. Then, when the aircraft was brought into a steady, straight and level flight, the autopilot would be engaged by the pilot. The airspeed, V_0 and altitude, h_0 value at the instance of autopilot engagement was taken as the trim condition which the autopilot would need to maintain. Meanwhile, throttle level was maintained constant throughout the automatic flight period. Judging by the flight safety consideration, the pilot has full authority to decide when to disengage the autopilot and resume control over the aircraft.

In the previous section, computer simulations showed that three longitudinal LQG controllers (*Lon#1*, *Lon#2* and *Lon#3*) display similar performance while one lateral LQG controllers, *Lat#1* outperforms the others. Hence, all three longitudinal controllers were tested in the flight tests while only one lateral controller was assessed. Samples of the flight test results are shown in Fig. 17 and Fig. 18. Note that in order to facilitate comparison between manual and

https://doi.org/10.1017/S0001924000002955 Published online by Cambridge University Press



(a) *Lon#2/Lat#1.* (b) *Lon#3/Lat#1.*

Figure 18. Flight test results of controllers.

automatic flight, so as to observe the effects of the autopilot on the aircraft's response, the aircraft was flown manually in the straight and level flight condition for approximately 10 seconds prior to the engagement of autopilot. The two thick lines demarcate the period when the autopilot was engaged.

Figure 17 corresponds to the responses of aircraft under the control of autopilot which consists of controllers *Lon#1* and *Lat#1*. The associated trim conditions were V_0 = 111·6km/h and h_0 = 135·1m. Overall, all aircraft states settled into steady state condition around the vicinity of trim values shortly after the autopilot was engaged (see Fig. 17). In particular, the performance output of the longitudinal motion, i.e. the altitude, h stayed at a value of approximately 137·5m which was within an error margin of less than 3m from the trim altitude, h_0. The airspeed, V although having a steady state error of about 5km/h, was able to remain constant around 105km/h while the pitch angle was contained within ±5deg throughout the automatic flight. This is an encouraging outcome since there is only one control input for the longitudinal motion, which implies that perfect tracking is only possible for one output variable. The lateral controller performed equally well judging from the successful regulation of the

https://doi.org/10.1017/S0001924000002955 Published online by Cambridge University Press

bank angle. Note that the spikes appeared in the measurements of the airspeed and altitude are caused by the noises associated with the air data sensors. They are also the culprit behind the similar spikes in the autopilot control commands. However the overall performance of the autopilot does not seem to be significantly affected.

In addition, the effect of the autopilot is clearly shown by comparing the aircraft's responses before and after the switch to automatic flight. Although the pilot is able to fly the aircraft in a stable and straight manner relative to human eyes, the output measurements suggest otherwise. The airspeed and altitude of the aircraft were observed to be varying gradually where h, in particular may vary as much as 20m. The attitudes of the aircraft, i.e. pitch and bank angles were not even close to the trim values. With the distinctively higher rate of controls, the aircraft's responses were rapidly regulated after the autopilot took over.

The flight test results of the other two longitudinal controllers, *Lon#2* and *Lon#3* were equally encouraging as shown in Fig. 18. Note that the angular rate measurements are excluded for simplicity. The regulation of the air data and aircraft attitudes is comparable to those of controller *Lon#1* (Fig. 17). The major difference among the three controllers lies in the amount of control efforts (elevator) required to achieve the regulation. It is found that the disparity matches the simulation results depicted in Fig. 15 where controller *Lon#3* uses the least control efforts compared with the other two controllers.

6.0 CONCLUDING REMARKS AND FUTURE WORK

The research effort presented in this paper focuses on the design and implementation of a stability augmentation autopilot based on the linear-quadratic-Gaussian (LQG) control law. The autopilot consists of two independent controllers which govern the longitudinal and lateral motion of the aircraft respectively. The longitudinal and lateral LQG controllers are designed separately using a simple and straight forward design procedure that makes use of convenient modern software packages, i.e. MATLAB®. In addition, this paper also demonstrated that it is highly feasible and beneficial to use the system identification routine based on two well-established identification methods, namely the subspace method and the prediction error method to obtain the aircraft linear models required for the autopilot design. Furthermore, the authors proposed to use the norm as the performance index which is shown to be a consistent parameter to assess the performance of different identified models. It is found to be an effective tool to evaluate the quality of models identified from different flight test data, especially when there is a large amount of data sets to be processed. Using the Spoonbill UAV as the research platform, consistent computer simulations and flight tests yielded encouraging results which verified the feasibility and the effectiveness of the LQG autopilot design synthesis proposed in this paper. One of the most attractive features about the design procedure is that it is readily applicable to any other UAV system as long as the air vehicle of interest is of conventional, fixed-wing configuration.

Without going into further elaboration, some of the major outcomes of this paper are listed in the following:

- successfully designed and built from the scratch, a structurally simple, stable and efficient unmanned aircraft.
- developed hardware and software of an onboard avionics system capable of performing data acquisition task and automatic flights.
- developed an interactive ground control station software which enables the real-time, continuous data-link communication between the airborne UAV and the ground operating personnel.
- established a complete system identification routine to obtain linear aircraft model which include a MATLAB®-based simple identification algorithm.
- developed a simple and straight forward LQG autopilot design procedures where the optimal controller gains are automatically generated by the design algorithm.
- demonstrated that a control-loop update rate of 10Hz is adequate for UAV to perform automatic flight.
- successfully validated the LQG stability augmentation autopilot in both computer simulations and actual flight tests.

The works presented in this paper formed a solid foundation for the Spoonbill UAV to realise fully automatic flight in the near future. Spoonbill project is an ongoing research effort where there are a lot of challenges and obstacles ahead. First and foremost, the aircraft models may be further refined by improving the fidelity and accuracy of the sensor measurement. More works are also foreseen in the issues of measurement noise reduction. This ought to be progressing in parallel with the improvement of the onboard avionics system, in terms of upgrading hardware devices and composing more efficient programming codes. Nevertheless, the encouraging progress made on the LQG regulator proved that it is feasible to extend the stability augmentation autopilot into a tracking controller. This means that it is possible for the UAV to perform beyond visual range, long endurance flight, based on Global Positioning System (GPS) navigation and guidance. The ultimate goal is to use the Spoonbill UAV system as a long term research platform in the quest to realise a truly intelligent UAV system that possesses the highest level of autonomy, adaptability to system failure or environmental uncertainties which require the least, if not none of human intervention in process of the entire flight mission.

ACKNOWLEDGEMENT

This work is supported by National Cheng Kung University, Taiwan, ROC under grant number, D97-3340 and D98-3340.

REFERENCES

1. Office of the Secretary of Defense, 2007, Unmanned Systems Roadmap, 2007-2032, Technical Report, OSD, US.
2. Office of the Secretary of Defense, 2005, Unmanned Aircraft Systems (UAS) Roadmap, 2005-2030, Technical Report, OSD, US.
3. MONTGOMERY, P.Y. Carrier Differential GPS as a Sensor for Automatic Control, PhD thesis, 1996, Stanford University.
4. CHO, A., KIM, J., LEE, S., CHOI, S., LEE, B. and KIM, B. Fully automatic taxiing, takeoff and landing of a UAV only with a single-antenna GPS receiver, Proceedings of AIAA Infotech@Aerospace 2007 Conference and Exhibit, Rohnert Park, California, USA.
5. JANG, J.S. and TOMLIN, C.J. Autopilot design for the Stanford DragonFly UAV: Validation through hardware-in-the-loop simulation, Proceedings of the AIAA Guidance, Navigation and Control Conference, 1999.
6. JANG, J.S. and TOMLIN, C.J. Longitudinal stability augmentation system design for the DragonFly UAV using a single GPS receiver, Proceedings of the AIAA Guidance, Navigation and Control Conference, Austin, AIAA-2003-5592, August 2003.
7. JANG, J.S. Nonlinear control using discrete-time dynamic inversion Under input saturation: theory and experiment on the Stanford DragonFly UAVs, PhD thesis, Department of Aeronautics and Astronautics, Stanford University, 2003.
8. ALSWAILEM, S.I. Application of Robust Control in Unmanned Vehicle Flight Control System Design, PhD thesis, 2004, College of Aeronautics, Cranfield University.
9. NATESAN, K., GU, D.W., POSTLETHWAITE, I. and CHEN, J. Design of flight controllers based on simplified LPV model of an UAV, Proceedings of the 45th IEEE Conference on Decision and Control, San Diego, CA, USA, 13-15 December 2006.
10. ANDRIEVSKY, B. and FRADKOV, A. Combined adaptive autopilot for an UAV flight control, Proceedings of the 2002 IEEE International Conference on Control Applications, Glasgow, Scotland, UK, 18-20 September 2002.
11. CHAN, W.L., LEE, C.S., HSU, C.W., HU, Y.T. and HSIAO, F.B. Preliminary design and analysis of an endurance UAV, Proceedings of

https://doi.org/10.1017/S0001924000002955 Published online by Cambridge University Press

the 5th Taiwan-Indonesia Workshop on Aeronautical Science, Technology and Industry, Tainan, Taiwan, 13-16 November 2006.
12. HSIAO, F.B., LAI, Y.C., TENN, H.K., HSIEH, S.Y., CHEN, C.C. and CHAN, W.L. The development of an unmanned aerial vehicle system with surveillance, watch, autonomous flight and navigation capability, Proceedings of the 21st Bristol UAVSystems Conference, Bristol, UK, 2006.
13. HSIAO, F.B., HSIEH, S.Y., CHAN, W.L. and LAI, Y.C. Engine speed and velocity controller development for small unmanned aerial vehicle, *J Aircr*, 2008, **45**, (2), pp 55-65.
14. LEE, C.S. The Realization of Optimal Stability Augmentation Autopilot for Unmanned Air Vehicle, Master Thesis, Institute of Aeronautics and Astronautics, National Cheng Kung University, Taiwan, 2008.
15. KLEIN, V. and MORELLI, E.A. Aircraft System Identification: Theory and Practice, 2006, American Institute of Aeronautics and Astronautics Education Series.
16. MORELLI, E.A. Estimating noise characteristics from flight test data using optimal fourier smoothing, *J Aircr*, July-August, 1995, **32**, (4), pp 689-695 .
17. VAN OVERSCHEE, P. and DE MOOR, B. *Subspace Identification of Linear Systems: Theory, Implementation, Applications*, 1996, Kluwer Academic Publishers.
18. STEVENS, B.L. and LEWIS, F.L. *Aircraft Control and Simulation*, 2nd ed, 2003, John Wiley & Sons.
19. BRYSON, A.E., Jr., and Ho. Y.–C. *Applied Optimal Control*, New York, USA, Hemisphere.LOUR

https://doi.org/10.1017/S0001924000002955 Published online by Cambridge University Press